Biochemistry

 Volume 37, Number 48 December 1, 1998

Accelerated Publications

Lowering the Entropic Barrier for Binding Conformationally Flexible Inhibitors to Enzymes[†,‡]

Amir R. Khan,[§] Jonathan C. Parrish,[§] Marie E. Fraser,[§] Whitney W. Smith,[||] Paul A. Bartlett,[||] and Michael N. G. James*[,§]

Department of Biochemistry, University of Alberta, Edmonton, Canada T6G 2H7, and Department of Chemistry, University of California, Berkeley, California 94720-1460

Received September 3, 1998

ABSTRACT: The design of inhibitors with enhanced potency against proteolytic enzymes has many applications for the treatment of human diseases. In addition to the optimization of chemical interactions between the enzyme and inhibitor, the binding affinity can be increased by constraining the inhibitor to the conformation that is recognized by the enzyme, thus lowering the entropic barrier to complex formation. We have structurally characterized the complexes of a macrocyclic pentapeptide inhibitor and its acyclic analogue with penicillopepsin, an aspartic proteinase, to study the effect of conformational constraint on the binding affinity. The phosphonate-based macrocycle PPi4 (K_i = 0.10 nM) is covalently linked at the P2-Asn and P1′-Phe side chains [nomenclature of Schechter and Berger, *Biochim. Biophys. Res. Commun.* (1967) *27*, 157−162] via an amide bond, relative to the acyclic compound PPi3 (K_i = 42 nM). Comparisons of the high-resolution crystal structures of PPi4-penicillopepsin (0.95 Å) and PPi3-penicillopepsin (1.45 Å) reveal that the conformations of the inhibitors and their interactions with the enzyme are similar. The 420-fold increase in the binding affinity of PPi4 is attributed to a reduction in its conformational flexibility, thus providing the first rigorous measure of the entropic contribution to the binding energy in a protein−ligand complex and stressing the advantages of the design strategy.

Proteolytic enzymes are involved in diverse biological processes, ranging from the digestion of dietary proteins to tumor invasion and cellular differentiation (*1*, *2*). The aspartic proteinases are a class of proteolytic enzymes that are attractive targets for inhibitors as a consequence of their role in human pathogens such as human immunodeficiency virus-1 (HIV-1 protease), malarial parasites (plasmepsins), and the fungus *Candida albicans* (*3*−*5*). Also, the enzyme renin is involved in the upregulation of blood pressure and has been a candidate for anti-hypertensive drugs in the past (*6*).

The overall structures of viral and cellular aspartic proteinases are conserved across the evolutionary spectrum. The structure of penicillopepsin from the fungus *Penicillium janthinellum* resembles a bilobate croissant shape and is composed of two β-barrel domains that are connected by a centrally located six-stranded β-sheet (Figure 1). The two

[†] This work was supported by a grant to the MRC Group in Protein Structure and Function, and by Grant MRC MT-12831, both from the Medical Research Council of Canada. P.A.B. was supported by grant GM-30759 from the National Institutes of Health.

[‡] The coordinates (and structure factors) have been deposited in the Brookhaven Protein Data Bank with accession codes 1bxo (r1bxosf) and 1bxq (r1bxqsf).

* To whom correspondence should be addressed. Phone (403) 492-4550. Fax (403) 492-0886. E-mail: michael.james@ualberta.ca.

[§] Department of Biochemistry, University of Alberta.

[||] Department of Chemistry, University of California.

10.1021/bi9821364 CCC: $15.00
Published on Web 11/11/1998

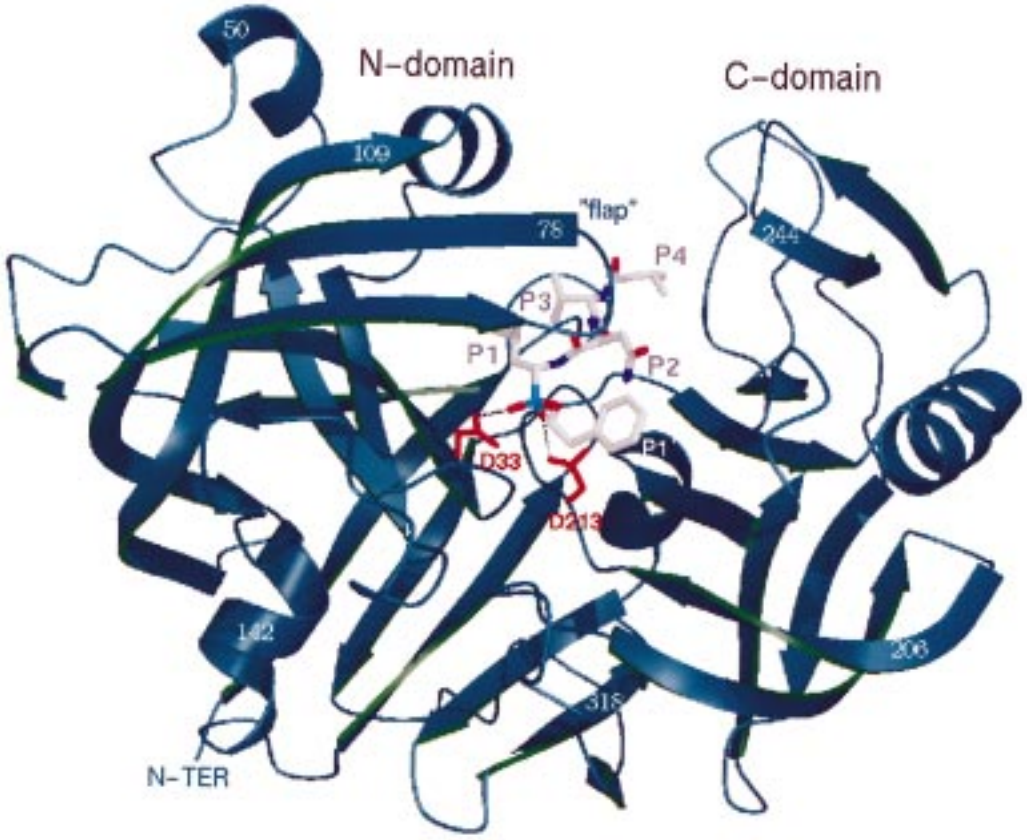

FIGURE 1: Ribbon drawing of the PPi3-penicillopepsin complex. The inhibitor is shown as a gray stick model. The side chains of the catalytic aspartates are red. The dashed lines represent hydrogen bonds between the phosphonate of the inhibitor and the Asp residues. The atoms of the C-terminal methyl ester [$-C(O)OCH_3$] of the inhibitor have been omitted for clarity. The figures were drawn using BOBSCRIPT (*31*) and RASTER3D (*32*).

catalytic aspartate residues, Asp^{33} and Asp^{213}, reside on two similarly folded loops at the base of the substrate-binding hydrophobic groove and in front of the central β-sheet. The structures of active enzymes contain a catalytic water between the aspartates that becomes deprotonated to initiate the general acid−base-catalyzed hydrolysis (*7*, *8*). The hydroxyl ion subsequently attacks the carbonyl-carbon atom of the scissile peptide bond between P1 and P1′ of substrates, thus forming a noncovalently bound tetrahedral transition-state intermediate along the reaction pathway.

Previous crystallographic studies of the phosphonate-containing inhibitor PPi2[1] (Figure 2) revealed that the competitive inhibitor binds in a β-strand-like fashion across the catalytic cleft of penicillopepsin (*9*). The phosphonate moiety of PPi2 displaces the nucleophilic water that is located between the catalytic aspartates, Asp^{33} and Asp^{213}, in the active enzyme (*10*). In addition, the tetrahedral geometry at the phosphorus atom resembles the cleavage transition state of the scissile carbonyl-carbon atom that is expected to form during peptide hydrolysis. As a consequence of the extended conformation of PPi2, alternating pairs of side chains (e.g., P2 and P1′) were sufficiently close together in space to prompt the design of covalent bridges (*11*). This strategy was first proposed in the context of the aspartic proteinases by Blundell and co-workers to improve the potency and selectivity of renin inhibitors (*12*). Macrocyclic conformational constraint shows particular promise for peptidomimetic drug design, since the affinity can be enhanced without substantially increasing molecular weight or hydrophobicity.

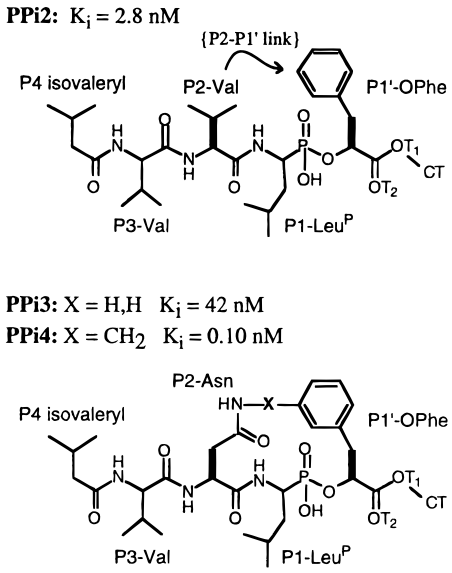

FIGURE 2: Chemical structures of the cyclic and acyclic pentapeptide inhibitors. The corresponding K_i values are shown, as determined previously (*9*, *11*).

The program CAVEAT (*13*) was used to identify structural frameworks linking the P2 and P1′ side chains, based on the structure of PPi2-penicillopepsin. The various possibili-

[1] Abbreviations: PPi, penicillopepsin phosphonate-based inhibitor; kDa, kilodaltons; rmsd, root-mean-square deviation; nM, nanomolar; NMR, nuclear magnetic resonance.

ties were evaluated by energy minimization and modeling procedures. The strategy suggested that changing P2-Val → P2-Asn, followed by attachment of the Asn side chain to P1′-Phe via an amide bond and a methylene group, would constrain the P2-P1′ segment of the inhibitor without perturbing the enzyme−inhibitor complex. The second-generation inhibitors PPi3 and PPi4 (Figure 2), differing by a single carbon atom, were therefore synthesized in order to evaluate the effect of this design strategy on inhibitor binding affinity and to assess the entropic advantage of conformational constraint (*11*).

In this paper, we describe the refined crystal structures of PPi3 and PPi4 in complexes with penicillopepsin. The remarkable similarity between the two structures reflects the success of the design strategy and indicates that the effect of conformational flexibility on the binding affinity has been differentiated from other enthalpic and entropic contributions to complex formation.

MATERIALS AND METHODS

Crystallization and Data Collection. The macrocyclic peptide-based inhibitor PPi4 {methyl cyclo[(2*S*)-2-[[(1*R*)-1-(*N*-L-*N*-(3-methylbutanoyl)valyl-L-aspartyl)amino)-3-methylbutyl]hydroxyphosphinyloxy]-3-(3-aminomethyl)phenylpropanoate] lithium salt} and its acyclic derivative PPi3 were synthesized as published previously (*11*), and both inhibitors were soluble in aqueous solution. Penicillopepsin was obtained as a powder preparation from Professor T. Hofmann, University of Toronto. The enzyme and inhibitors were mixed in solution at a penicillopepsin:inhibitor molar ratio of 1:6, and the complexes were cocrystallized by the hanging drop method in 35% ammonium sulfate and 100 mM sodium acetate (pH 4.6) at a final protein concentration of 12 mg/mL. The pH of the crystallization buffer was identical to the pH employed during kinetic analyses of the inhibitors. Macro-seeding techniques were used to grow large crystals in the monoclinic space group C2, with one enzyme−inhibitor complex in the asymmetric unit.

Prior to data collection, crystals were transferred to a reservoir solution containing incremental amounts of glycerol up to a maximum of 25% (v/v). The crystals were flash frozen, and data were collected at 100 K from single crystals at either the Cornell High Energy Synchrotron Source (CHESS, PPi4-penicillopepsin) or in the laboratory (PPi3-penicillopepsin) using a Siemens rotating anode X-ray generator and X1000 multiwire area detector system. CHESS data were collected to a maximum of 0.90 Å resolution using a Quantum 2 × 2 CCD detector, processed with MOSFLM (*14*), and scaled using SCALA (*15*). Laboratory data were collected to a maximum resolution of 1.41 Å at 110 K, and processed with XENGEN software (*16*).

Refinement of Structures. Prior to structure determinations, a random selection of 10% of the reflections were flagged as the *R*-free set and were excluded from the refinement process. The structures were refined using PPi2-penicillopepsin (PDB code 1ppl) as the starting model, devoid of all water and inhibitor atoms. The starting *R*-factors were about 40% for data between 8 and 2.5 Å resolution, and electron density maps clearly identified all atoms corresponding to the inhibitors PPi3 and PPi4. Both complexes were initially refined using X-PLOR, and atomic models were adjusted using the programs O or XtalView (*17, 18*). In the latter stages of refinement, the program SHELX-97 (*19*) was used to perform several rounds of restrained conjugate-gradient least-squares (CGLS) minimization of the structures against diffraction intensities (10 cycles/round), with model building after each round. In the case of PPi4-penicillopepsin, anisotropic *B*-factor refinement (SHELX-97) was implemented using all data between 10 and 0.95 Å resolution. The statistics of the data and refinement are shown in Table 1.

Table 1: Crystal Data and Refinement

	PPi3	PPi4 (CHESS)
space group		
a (Å)	96.24	96.98
b (Å)	46.47	46.65
c (Å)	65.38	65.71
β (deg)	115.58	115.57
X-rays' λ (Å)	1.5418 Å	0.919 Å
detector	Siemens image plate detector	2×2 Quantum CCD detector
resolution (Å)	1.45	0.95
measurements	107 304	430 728
unique reflections	45 997	156 181
no. of parameters	11 596	27 767
R_{merge}[a]	7.4%	5.3%
completeness,	94.8 (8−1.44 Å)	98.0 (10−0.95 Å)
	66.3 (1.46−1.44 Å)	51.7 (0.97−0.95 Å)
$F/\sigma(F) > 3.0$	56.4 (1.46−1.44 Å)	39.1 (0.97−0.95 Å)
R_{cryst} (%)[b]	14.5	9.91
R_{free} (%)	18.4	12.47
models		
protein residues	1−323	1−323
inhibitor atoms	43	44
waters	412	491
sulfate ions	2	2
glycerol molecules	2	2
rms deviations in angstrom (SHELX-97)		
bond lengths	0.010	0.017
1,3 distances	0.029	0.034
Ramachandran map		
most favored	93.3%	91.0%
additional regions	6.7%	9.0%

[a] $R_{merge} = \sum_{hklj}|I_{hklj} - \langle I_{hkl}\rangle|/\sum_{hklj}\langle I_{hkl}\rangle \times 100\%$. [b] $R = \sum||F_o| - |F_c||/\sum|F_o| \times 100\%$.

RESULTS

The structure of PPi3-penicillopepsin reveals that the inhibitor is positioned in the substrate cleft that is between the N- and C-terminal domains of penicillopepsin (Figures 1 and 3). The complex is stabilized by extensive hydrogen-bonding and hydrophobic interactions that bury ~80% of the solvent-accessible surface area of PPi3 (Tables 2 and 3). The phosphonyl moiety of PPi3 resides between the catalytic aspartate residues, Asp^{33} and Asp^{213}, with the *pro-S* oxygen atom (POH) of the phosphonate group making a short (2.39 Å) hydrogen bond to the Oδ1 atom of Asp^{33}. The length and stereochemistry of this hydrogen bond is consistent with a symmetric single-well potential energy function for the hydrogen (*9*). The "flap" in the aspartic proteinases is a β-hairpin loop (in penicillopepsin, residues 71−82) that forms a wall against which the inhibitor packs on the opposite side of the cleft from the catalytic Asp residues. The side chain of Tyr^{75} in the flap forms part of the S1 pocket, and this residue is conserved in all cellularly derived aspartic

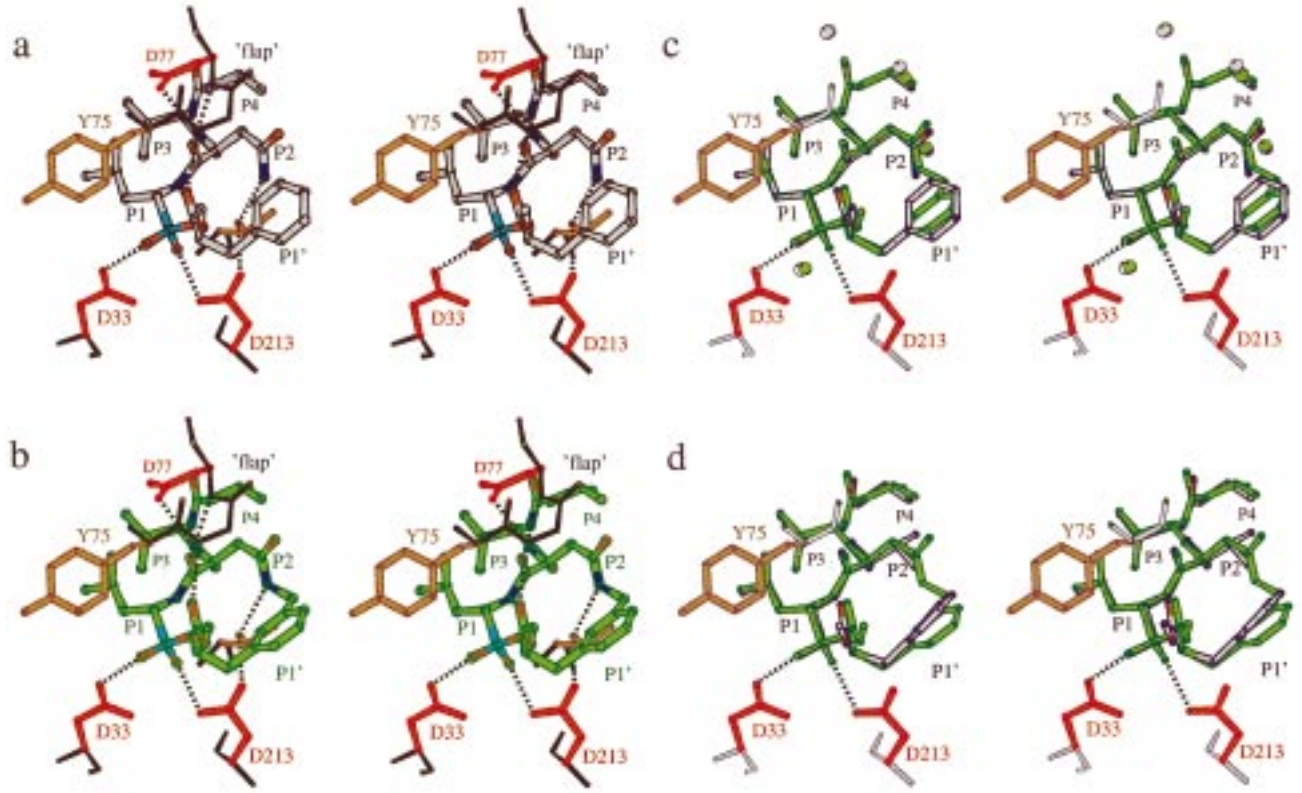

FIGURE 3: Stick models of cyclic and acyclic peptide inhibitors at the active site, shown in divergent stereo. (A) Structure of PPi3-penicillopepsin. The carbon skeleton of PPi3 is gray, oxygen atoms are red, nitrogens are blue, and the phosphorus atom is cyan. The catalytic Asp residues (red) form hydrogen bonds with the phosphonate moiety of the inhibitor. The side chain of Thr^{216} (brown) is involved in the network of hydrogen bonds in the vicinity of the phosphonate. Tyr^{75}, located in the flap region, forms part of the S1 hydrophobic pocket and interacts with P1-Leu. The flap (black) also contributes hydrogen bonds from the backbone NH of Gly^{76}, NH of Asp^{77}, and Oδ1 of Asp^{77}. (B) Structure of PPi4-penicillopepsin. The coloring scheme is similar, except that the carbon atoms and bond vectors of the inhibitor are green. The P2−P1′ side chains of PPi4 are bridged by an amide bond and a methylene carbon. (C) Comparisons of the structures of PPi3 (grey) and PPi4 (green). The superposition was performed using the enzyme backbone, thus excluding the inhibitors from the calculation. The flap and the active site aspartates correspond to PPi3. Thr^{216} and most of the flap residues have been omitted to show the superimposed inhibitors clearly. Four conserved water molecules are shown as gray (PPi3) and green (PPi4) spheres. (D) Superposition of the structures of PPi2 (grey) and PPi4 (green). The enzyme backbone atoms were used in the calculation, and the inhibitor atoms were excluded. The flap and the active site aspartates are from PPi2.

Table 2: Hydrogen-Bonding Contact Distances Between Phosphonate Inhibitors and the Enzyme

	atoms[a]		distances (Å)		
site	inhibitor	enzyme	PPi2	PPi3	PPi4
P3	CO	Thr217 (NH)	3.03	3.04	3.05
	NH	Thr217 (Oγ1)	2.88	3.15	2.94
P2	NH	Asp77 (Oδ1)	2.93	2.83	2.89
	Nδ2 (Asn)	Thr216 (Oγ1)		2.97	3.02
	CO	Asp77 (NH)	3.00	3.09	3.14
P1	NH	Gly215 (O)	3.22	3.03	3.06
	POH[b]	Asp33 (Oδ1)	2.40	2.39	2.42
	PO	Asp33 (Oδ2)	3.21	3.16	3.17
	PO	Asp213 (Oδ1)	2.60	2.51	2.54
P1′	OT2 (ester)	Gly76 (NH)	2.89	2.95	2.92

Side-Chain Rotamers of P1′-Phe
PPi2 (χ1, χ2) = (62°, −82°)
PPi3 (χ1, χ2) = (73°, −37°)
PPi4 (χ1, χ2) = (67°, −73°)

[a] The estimated coordinate accuracy for the complexes of PPi2 (*9*) and PPi3 is estimated to be <0.1 Å from the method of Luzzati (*34*). Positional estimated standard deviations from the inverted matrix of unrestrained blocked-matrix least-squares refinement in SHELX-97 are less than 0.01 Å for atoms at the active site of PPi4-penicillopepsin. [b] Corresponds to the low-barrier hydrogen bond.

Table 3: Solvent-Accessible Surface Area (Å^2)[a]

	uncomplexed			complexed			
inhibitor[b]	polar	apolar	total	polar	apolar	total	% buried
PPi2[c]	192	673	866	26	124	150	83
PPi3	256	628	880	38	123	161	82
PPi4	245	636	881	40	121	161	82

[a] Calculated using the algorithm of Richards (*35*), as implemented by the program of Connolly (*36*, *37*). [b] The PDB files were first stripped of water molecules. [c] PDB code 1ppl.

proteinases. The tip of the flap makes two main-chain hydrogen bonds via the backbone nitrogen (NH) atoms of Gly^{76} and Asp^{77} with PPi3, further clamping the inhibitor to the active site. The extended conformation of PPi3 brings the side-chain atoms Nδ2 of P2-Asn and Cϵ1 of P1′-Phe to within 3.43 Å (Figure 3).

The rationally designed macrocycle PPi4 is a very potent inhibitor of penicillopepsin (K_i = 0.10 nM). The complex PPi4-penicillopepsin was refined using data to 0.95 Å resolution, with excellent agreement between observed and calculated structure factors (R_{cryst} = 9.91%, R_{free} = 12.47%). The quality of the data is unprecedented given the 35 kDa size of the protein (Figure 4), and a detailed structural analysis will be provided elsewhere. Crystals of PPi3-penicillopepsin are also exceptional, and future studies will involve characterization of this complex beyond 1.0 Å

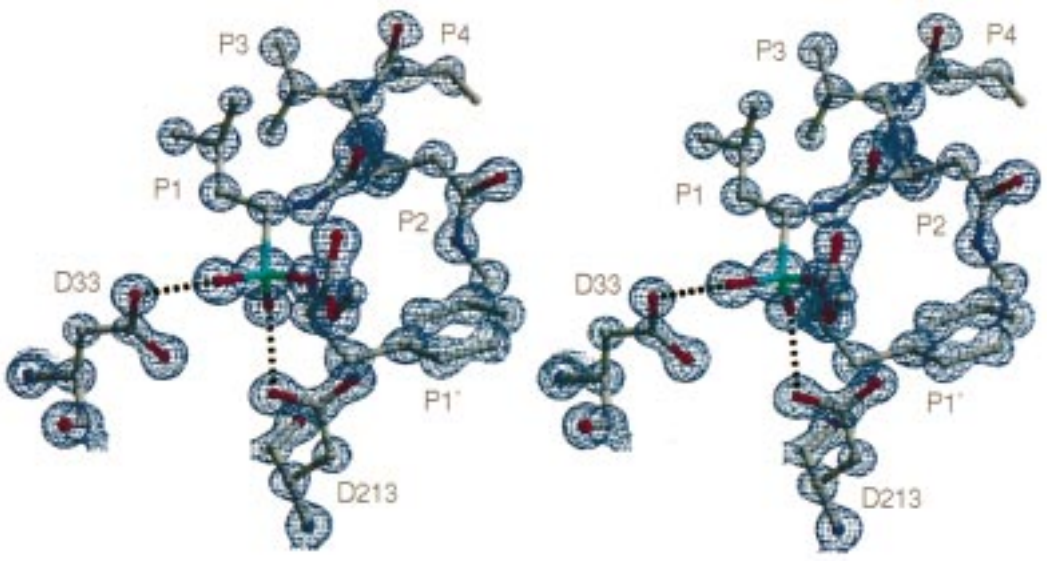

FIGURE 4: Electron density at the active site region of the refined model of PPi4-penicillopepsin. The map is contoured at 2.0σ, revealing the density around single atoms. Many hydrogen positions are also observed in difference electron density maps.

Table 4: Least-Squares Superpositions of Enzyme-Inhibitor Complexes[a]

	PPi2	PPi3	PPi4
PPi2		0.30 (1260)	0.28 (1260)
PPi3	0.25 (34)		0.19 (1260)
PPi4	0.30 (34)	0.17 (37)	

[a] The values given are rms deviations in angstrom units. The upper right portion of the matrix is a superposition of the enzyme backbone. Residues 1−2, 278−281, and 322−323 were disordered and therefore excluded from the calculations. The bottom left region of the matrix is a superposition of the inhibitor atoms. The P1′-Phe ring atoms were excluded from these calculations. The numbers in brackets indicate the number of common atoms used in the superposition.

resolution. Although many alternate conformations are observed for both PPi4-penicillopepsin (30 residues) and PPi3-penicillopepsin (12 residues), it is important to note that they occur in regions remote from the active site and do not affect the discussions below.

As predicted by the design strategy, the position and conformation of PPi4 in the complex with penicillopepsin is virtually identical to PPi3 (Figure 3). Comparisons of the hydrogen bond distances, the surface areas buried in the complexes, and the root-mean-square (rms) deviations of the enzyme and inhibitor reveal very similar binding of these two inhibitors (Tables 2−4). The most pronounced conformational difference between PPi4 and PPi3 is a 36° rotation at the χ2-angle of P1′-Phe. In PPi4-penicillopepsin, χ2 adopts a favorable value of −73° (*20*), whereas the P1′-Phe side chain of PPi3 is rotated to a χ2-value of −37°. Rotation of the phenyl ring in PPi3 is likely due to the close approach of the side chain of P2-Asn. The side chain of P2-Asn is firmly held in its position by a hydrogen bond between the Nδ2 atom and Oγ1 of Thr[216] in both PPi3 and PPi4. In the cyclic PPi4 structure, the P1′-Phe(Cϵ1) atom is situated 2.52 Å from Nδ2 of P2-Asn because of the methylene group that binds them together; direct replacement of the methylene group with two hydrogens, thus forming acyclic PPi3, would lead to a severe steric clash were the phenyl ring not rotated slightly, as observed in Figure 3c.

The largest atom coordinate difference between the two inhibitors is 1.29 Å (Cϵ1 of P1′-Phe) after superposition of the penicillopepsin backbone. The positions of the atoms of penicillopepsin that form the substrate clefts in the two complexes are identical despite the conformational change observed at P1′-Phe. In addition, 11 of 13 water molecules in the vicinity of PPi3 (<4.0 Å) have structural equivalents in the complex of PPi4-penicillopepsin. Upon superposition of the enzyme backbone, the rms deviation of these 11 waters is 0.31 Å.

The complexes of PPi3 and PPi4 with the enzyme can be compared to the 1.8 Å structure of PPi2-penicillopepsin (K_i = 2.8 nM), the parent complex from which the inhibitors were designed (Tables 2−4, Figure 3d). The chemical interactions and the surface areas buried in the three structures are similar. However, PPi2 is more hydrophobic as a consequence of the valine residue at P2, which also permits the χ2-angle of P1′-Phe to adopt a favorable value of −82° without steric clashes. The gain in hydrophobic interactions is tempered by the lack of a side-chain hydrogen bond to the enzyme relative to PPi3 and PPi4 (Table 2). The close structural similarities among the three enzyme−inhibitor complexes indicate that the attempt at rational design of PPi4 was successful. The 15-fold lower K_i of PPi2 relative to PPi3 (both of which are acyclic) may reflect the preference of the hydrophobic S2 pocket for P2-Val, thus contributing to enthalpic differences.

DISCUSSION

There are many enthalpic and entropic contributions to the binding of a peptide to a protein. For example, the entropic terms include the desolvation and rigidification of those residues in the ligand and the protein that mediate formation of the complex, as well as the loss of global rotational and translational degrees of freedom in the bimolecular association. In the complexes of PPi3- and PPi4-penicillopepsin, the similarities in the chemical interactions (hydrogen bonds, van der Waals contacts) and the amount

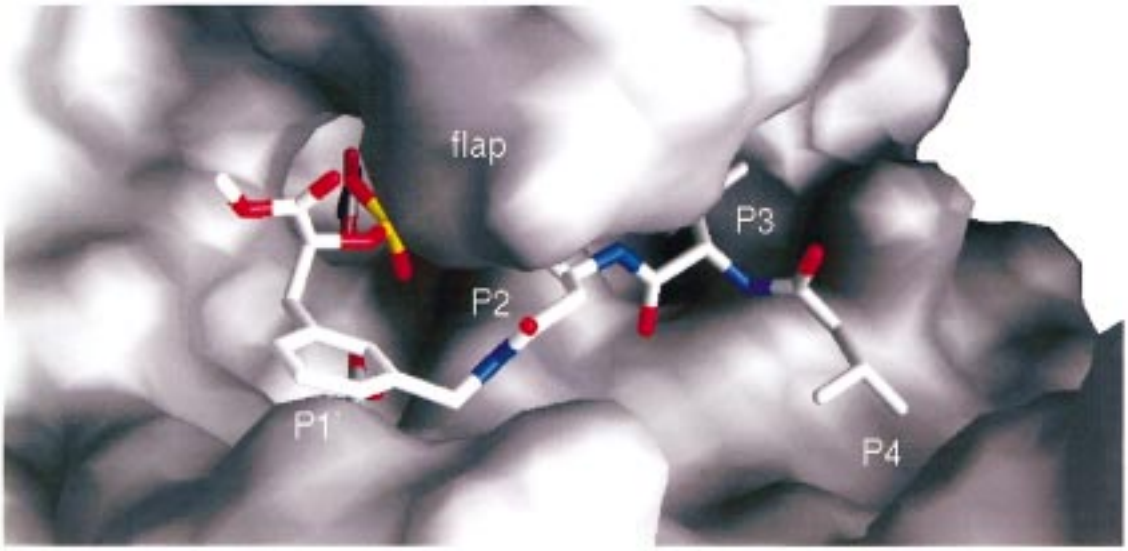

FIGURE 5: Molecular surface rendering of the active site of PPi4-penicillopepsin. The inhibitor is represented by stick vectors. The view has been rotated so that the extended conformation of PPi4 is horizontal, allowing a direct view into the active site cleft. The figure was drawn using GRASP (*33*).

of surface areas buried (82%) suggest that many of these energy terms are almost identical. There is only the slight movement of the phenyl ring at P1′-Phe that could represent a small enthalpic difference in their binding energies. It is apparent that the 420-fold difference in binding affinity between inhibitors PPi3 and PPi4 can mostly be attributed to the entropy that is associated with internal bond rotations. The overall free-energy difference is given by

$$\Delta\Delta G^\circ = -RT[\ln(K_{i,cyc}/K_{i,acy})] \quad (1)$$

where R is the universal gas constant, T is the temperature (in kelvin), and K_i is the inhibition constant (moles/liter) for the cyclic and acyclic inhibitors. The $\Delta\Delta G^\circ$ value of 3.6 kcal/mol derived from eq 1 represents the entropic penalty required to freeze out the enzyme-bound conformation from the flexible conformations of PPi3, relative to PPi4, during the binding process. The value of this penalty can also be estimated on a per-bond basis, as described previously (*11*). In our case, the 3.6 kcal/mol value corresponds to an average of 0.9 kcal/mol/degree of freedom due to bond rotations. This value is well within the range of 0.7−1.6 kcal/mol reported in the literature from studies of small molecules and the thermodynamic behavior of helix-forming peptides (*21*−*24*).

The conformation of PPi4 through the backbone closely resembles the solution structure that was proposed from a combined nuclear magnetic resonance (NMR) and modeling approach (*11*), suggesting that little distortion is required to form the complex. However, the two conformations differ significantly in the orientation of the amide linkage between P2-Asn and P1′-Phe; in the NMR model, it is flipped 180° relative to the crystal structure of the complex. The NMR-derived constraints were unable to distinguish between these two conformers, and the assignment was made on the basis of the relative energies predicted from the modeling. A reexamination of these modeling results reveals that the energy difference between the two conformers is highly dependent upon the force-field employed and may indeed be very small. When the alternative conformation of PPi4 is modeled into the active site, the Oδ1 atom of P2-Asn resides only 1.4 Å away from the Oγ1 atom of Thr^{216}, which would result in significant destabilization. Thus, the observed binding affinity for PPi4 would be reduced to the extent that an equilibrium between the two conformers exists in solution. In addition, the amide bond linking P2-Asn and P1′-Phe is distorted from an ideal plane by 11.2° at its equivalent ω-angle. Such a distortion from planarity corresponds to a cost of ∼1.0 kcal/mol (*25*) and, if it is induced on binding rather than forced by the macrocycle structure itself, may further decrease the binding affinity of PPi4. Together, these deviations from a perfect comparison of PPi3 and PPi4 suggest that the experimental value of 3.6 kcal/mol represents a lower limit to the entropic penalty for binding of PPi3 to penicillopepsin.

Previously, the structure of the parent PPi2-penicillopepsin complex suggested the feasibility of linking the side chains of P3-Val and P1-Leu. Accordingly, a macrocylic phosphonate inhibitor was synthesized in which the P3 and P1 side chains were linked by a naphthalene bridge (*26*). The structure of its complex with penicillopepsin was determined along with those of two acyclic analogues, the P1- and P3-naphthyl derivatives (*27*). The binding affinities within this series of inhibitors increased as the degree of conformational freedom decreased, also suggesting that the overall strategy had been successful. However, the structures of the enzyme−inhibitor complexes were sufficiently different to prevent attributing the differences in binding entirely to the flexibility of the inhibitors. In this respect, the success of the P2-P1′ inhibitors may reflect the peripheral location and less intrusive nature of the amide bridge linking the P2 and P1′ side chains (Figure 5).

Concluding Remarks. Entropy changes associated with molecular recognition are notoriously difficult to measure due to uncertainties in the entropy of the ligand in solution, as well as the residual motion of the ligand in the complex (*28*). Recently, macrocyclic inhibitors have been synthesized against proteolytic enzymes to enhance their potency and selectivity, but without a quantitative analysis of the effect (*29, 30*). In this study, the P2-P1′ macrocycle PPi4 represents the most rigorous and successful attempt to

differentiate the entropy of internal bond rotations from the remaining free-energy binding parameters in a large and complex system. The observed 420-fold increase in binding provides justification for pursuing this strategy in drug design, and is applicable to many other enzyme−inhibitor complexes. Clearly, further structural and thermodynamic studies would be required for more detailed analyses, such as a residue-specific entropy dependence. Such quantitative studies are a necessary step toward a better understanding of the forces that drive molecular recognition and accurate predictions of binding affinities (*28*).

ACKNOWLEDGMENT

The authors wish to thank Dr. Ashley Deacon for his expertise with data collection at CHESS. We are indebted to Dr. Theo Hofmann for supplying penicillopepsin.

REFERENCES

1. Edwards, D. R., and Murphy, G. (1998) *Nature 394*, 527−528.
2. Weinmaster, G. (1998) *Science 279*, 336−337.
3. Wlodawer, A., and Erickson, J. W. (1993) *Annu. Rev. Biochem. 62*, 543−585.
4. Cutfield, S. M., Dodson, E. J., Anderson B. F., Moody, P. C., Marshall, C. J., Sullivan, P. A., and Cutfield, J. F. (1995) *Structure 3*, 1261−1271.
5. Francis, S. E., Banerjee, R., and Goldberg, D. E. (1997) *J. Biol. Chem. 272*, 14961−14968.
6. Sielecki, A. R,. Hayakawa, K., Fujinaga, M., Murphy, M. E., Fraser, M., Muir, A. K., Carilli, C. T., Lewicki, J. A., Baxter, J. D., and James, M. N. G. (1989) *Science 243*, 1346−1351.
7. Suguna, K., Padlan, E. A., Smith, C. W., Carlson, W. D., and Davies, D. R. (1987) *Proc. Natl. Acad. Sci. U.S.A. 84*, 7009−7013.
8. James, M. N. G., Sielecki, A. R., Hayakawa, K., and Gelb, M. H. (1992) *Biochemistry 31*, 3872−3886.
9. Fraser, M. E., Strynadka, N. C. J., Bartlett, P. A., Hanson, J. E., and James, M. N. G. (1992) *Biochemistry 31*, 5201−5214.
10. James, M. N. G., and Sielecki, A. R. (1983) *J. Mol. Biol. 163*, 299−361.
11. Smith, W. W., and Bartlett, P. A. (1998) *J. Am. Chem. Soc. 120*, 4622−4628.
12. Blundell, T. L., Cooper, J., Foundling, S. I., Jones, D. M., Atrash, B., and Szelke, M. (1987) *Biochemistry 26*, 5585−5590.
13. Lauri, G., and Bartlett, P. A. (1994) *J. Comput.-Aided Mol. Design 8*, 51−66.
14. Leslie, A. G. W. MOSFLM Version 5.50, MRC Laboratory of Molecular Biology, University of Cambridge, U.K.
15. Evans, P. R. (1993) in *Data Reduction*, Proceedings of CCP4 Study Weekend on Data Collection and Processing, pp 114−122.
16. Howard, A. J. (1987) *J. Appl. Crystallogr. 20*, 383−387.
17. Jones, T. A., and Kjeldgaard, M. (1995) *O—the Manual*, Version 5.11, Uppsala, Sweden.
18. McCree, D. M. (1992) *J. Mol. Graphics 10*, 44−46.
19. Sheldrick, G. M. (1997) The SHELX-L 97 Manual, University of Gottingen, Germany.
20. Schrauber, H., Eisenhaber, F., and Argos, P. (1993) *J. Mol. Biol. 230*, 592−612.
21. Page, M. I., and Jencks, W. P. (1971) *Proc. Natl. Acad. Sci. U.S.A. 68*, 1678−1683.
22. Andrews, P. R., Craik, D. J., and Martin, J. L. (1984) *J. Med. Chem. 27*, 1648−1657.
23. Williams, D. H., Searle, M. S., Mackay, J. P., Gerhard, U., and Maplestone, R. A. (1993) *Proc. Natl. Acad. Sci. U.S.A. 90*, 1172−1178.
24. Gomez, J., and Freire, E. (1995) *J. Mol. Biol. 252*, 337−350.
25. MacArthur, M. W., & Thornton, J. M. (1996) *J. Mol. Biol. 264*, 1180−1195.
26. Meyer, J. H., and Bartlett, P. A. (1998) *J. Am. Chem. Soc. 120*, 4600−4609.
27. Ding, J., Fraser, M. E., Meyer, J. H., Bartlett, P. A., and James, M. N. G. (1998) *J. Am. Chem. Soc. 120*, 4610−4621.
28. Searle, M. S., and Williams, D. H. (1992) *J. Am. Chem. Soc. 114*, 10690−10697.
29. Ettmayer, P., Billich, A., Hecht, P., Rosenwirth, B., and Gstach, H. (1996) *J. Med. Chem. 39*, 3291−3299.
30. Ksander, G. M., de Jesus, R., Yuan, A., Ghai, R. D., McMartin, C., and Bohacek, R. (1997) *J. Med. Chem. 40*, 506−514.
31. Esnouf, R. M. (1997) *J. Mol. Graphics 15*, 133−138.
32. Merritt, E. A., and Murphy, M. E. P. (1994) *Acta Crystallogr., Sect. D 50*, 869−873.
33. Nicholls, A., Sharp, K. A., and Honig, B. (1991) *Proteins 11*, 281−296.
34. Luzzati, V. (1952) *Acta Crystallogr. 5*, 802−810.
35. Richards, F. M. (1977) *Annu. Rev. Biophys. Bioeng. 6*, 151−176.
36. Connolly, M. L. (1983) *Science 221*, 709−713.
37. Connolly, M. L. (1983) *J. Appl. Crystallogr. 16*, 548−558.

BI9821364